Technical Notes

TECHNICAL NOTES are short manuscripts describing new developments or important results of a preliminary nature. These Notes cannot exceed 6 manuscript pages and 3 figures; a page of text may be substituted for a figure and vice versa. After informal review by the editors, they may be published within a few months of the date of receipt. Style requirements are the same as for regular contributions (see inside back cover).

Laser Gain Measurements in a Long Noncontoured Hypersonic Nozzle

M. A. S. Minucci*
Centro Técnico Aeroespacial, São José dos Campos, Brazil
and
J. N. Hinckel†
Instituto de Pesquisas Espaciais, São José dos Campos, Brazil

Introduction

THE performance of gas dynamic lasers is proportional to the population inversion created by the nonequilibrium expansion of the lasing gas through a nozzle. The population inversion is characterized by the small-signal gain coefficient G_0. Previous studies measured G_0 in constant area ducts located downstream of minimum length contoured nozzles.[1-3] Some of these studies have reported departures from theory at large distances from the nozzle throat ($200h^*$). Such departures have been attributed to viscous effects and weak shock patterns existing in constant area ducts. These observations and the interest in evaluating the nonequilibrium expansion of the CO_2-N_2-He system in a long, noncontoured nozzle motivated this investigation. By measuring the gain during the gas expansion in the supersonic section of the nozzle, the deleterious effects of shock wave patterns on G_0 were avoided. The viscous effects on G_0 were minimized through the use of relatively high characteristic Reynolds numbers Re_0.[4]

A shock tube[1,5,6] is used to provide a reservoir of hot, highly pressurized, vibrationally excited gas for subsequent expansion through the nozzle. A nonequilibrium population inversion is created when this shock-heated[7] gas expands through a double-wedge type nozzle mounted at the end of the shock tube.

Small-signal gain measurements are made at three different locations along the nozzle centerline for different reservoir conditions. Good agreement between experimental data and the analytical model was observed at the two first stations near the nozzle throat. At the station near the exit of the nozzle, the experimental results are below the theoretical curves.

Analytical Models

The nonequilibrium flow model developed by Glowacki and Anderson[8] was used. The model assumes a simplified vibrational kinetic mechanism for CO_2-N_2 and an inviscid one-dimensional flow of a thermally perfect gas in a supersonic nozzle. The original computer code version used H_2O as a catalyst and had to be modified[9] for use with He.

The temperature and pressure of the shock-heated gas is determined analytically[9] by solving Euler's equations in the region between the reflected shock wave and the nozzle throat. The solution of these equations is obtained assuming a choked flow at the nozzle throat and an equilibrium flow up to that location. The incident shock wave velocity and initial driven conditions are experimentally determined. The reservoir pressure is measured in every experiment and compared to the analytical one. The agreement is within 3%.

Experimental Apparatus

The shock tube used[9] is 70 mm in diameter; helium was used as the driver gas at pressures ranging from 5 to 65 atm. The driver tube was separated from the driven tube by a 0.5-mm-thick diaphragm. A commercial mixture of 6.6% CO_2, 54.1% N_2, 39.3% He was used as the test gas. The driven tube pressures were in the 20–60 mm Hg range. At the end of the shock tube, the driven section is separated from the hypersonic nozzle entrance by a scored Mylar diaphragm 0.025 mm thick. The nozzle exhausts into an evacuated (less than 10^{-1} Torr) dump tank in order to shorten the flow establishment time. Two ports in the driven tube, near the nozzle section, are instrumented with quartz piezoelectric pressure transducers. The one closer to the nozzle is used for determining the shock-heated gas pressure. A time interval counter connected to both pressure transducers (31.5 cm apart) measured the incident shock wave transit time. The shock tube was capable of generating reservoir pressures from 2 to 27 atm and reservoir temperatures from 800 to 2700 K. The useful test time was of the order of 300 μs.

A two-dimensional double wedge (sharp throat) nozzle was used to drive the nonequilibrium expansion of the gas mixture. The nozzle area ratio was 53 and the throat height h^* was 1.25 mm. The hypersonic section of the nozzle is 230 mm long; the subsonic portion is 3 mm long to improve the freezing of the CO_2-N_2 upper level. The stainless steel nozzle walls have a very good surface finishing to minimize flow disturbances. To permit G_0 measurements, the nozzle has three pairs of ports (35 mm in diameter) centered at 72, 130, and 187 mm downstream from the throat (Fig. 1). To minimize flow disturbances, the antireflection coated Ge windows are flush with the inner sidewall surfaces.

The gain coefficient was determined by measuring the increase in power of the probe beam between no flow and flow. The diagnostic laser is provided by a homemade CO_2 CW gas laser operating at 10.6 μm predominantly on the P(20) transition. The intensity was 0.1 W/cm^2, which is below the saturation intensity of the medium (1.0 kW/cm^2). The beam is mechanically chopped and then injected into the nozzle flow. After passing through the nozzle, the probe beam is diffused by reflection from a rough-surfaced aluminum plate to ensure coverge of the active area (1 mm^2) of the N_2/ cooled HgCdTe detector. Both the infrared detector and the pressure signals are recorded by a digital oscilloscope. Then G_0 is determined from the expression $G_0 = (1/L)\ln I_{after}/I_{before}$, where L is 70 mm (nozzle width), and I_{before} and I_{after} are, respectively, the measured diagnostic laser beam intensities before and after crossing the active medium.

Presented as Paper 90-1511 at the AIAA 21st Fluid Dynamics, Plasma Dynamics and Lasers Conference, Seattle, WA, June 18-20, 1990; received July 19, 1990; revision received Oct. 2, 1990; accepted for publication Oct. 4, 1990.

*1st Lieutenant, Brazilian Air Force; currently Graduate Student, Rensselaer Polytechnic Institute, Troy, NY. Student Member AIAA.
†Senior Research Scientist.

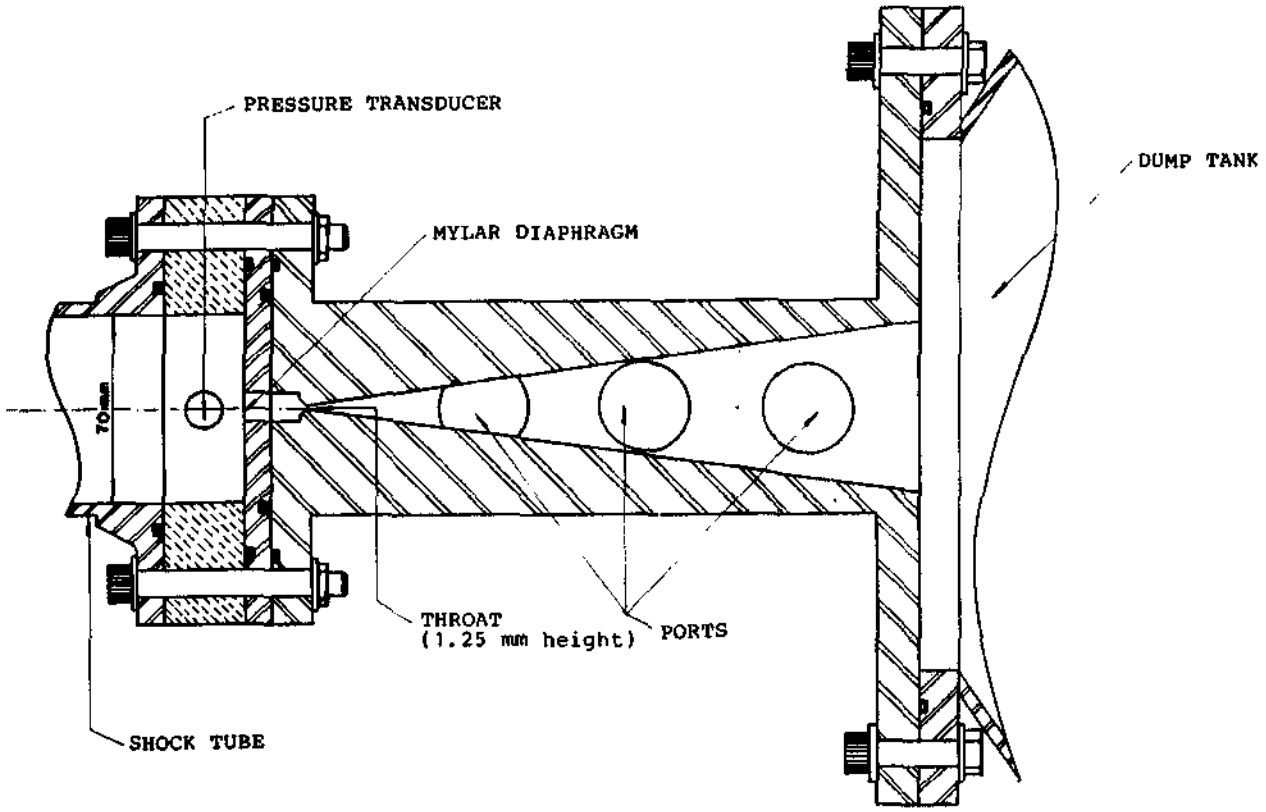

Fig. 1 Double-wedge nozzle and cavity arrangement.

Table 1 Test conditions and important parameters

Test no.	p_0, atm	T_0, K	p_0h^*, atm-cm	$Re_0 \times 10^5$	$G_{0,m}$, (m^{-1})
1	12.0	2000	1.50	0.7	0.91
2	13.5	1445	1.69	1.1	0.78
3	7.0	1500	0.88	0.6	0.88
4	23.0	1620	2.88	1.7	0.89
5	10.0	1820	1.25	0.6	0.94
6	11.0	1000	1.34	1.4	0.38

Results

Table 1 lists the reservoir pressure and temperature p_0 and T_0, the binary scale parameter p_0h^*, the characteristic Reynolds number[4] Re_0, and the measured peak gain values $G_{0,m}$.

According to Mitra and Fiebig,[4] the viscous losses on the small-signal gain are negligible when Re_0 is of the order of 10^5. From Table 1 it is seen that, for all of the test conditions, the characteristic Reynolds number is of the order of 10^5. Furthermore, due to the short duration of the flow, the cold wall assumption is valid. Such facts lead to the existence of very thin boundary layers. Under these circumstances, the viscous effects are highly attenuated. Another important observation is that the nozzle flow is shock-free. The reasons are 1) the continuous expansion of the gas in the double wedge type nozzle and 2) the back pressure in the dump tank being many times smaller than the nozzle exit pressure.

The measured small-signal gain profiles along the nozzle centerline and the computed values are shown in Figs. 2 and 3 for the conditions listed in Table 1. These figures show that the largest departures between theory and experiment occur far downstream from the nozzle throat. The best agreement in that region occurred when the lowest reservoir temperature (1000 K) was used (Fig. 3). For this case, the theory shows a decrease in the gain at points located far downstream from the nozzle throat. Such a trend is not observed in the other cases

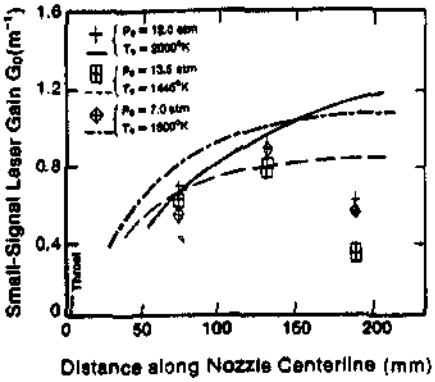

Fig. 2 Comparison between theoretical (lines) and experimental (points) small-signal laser gain profiles.

where higher temperatures were used. Since viscous and shock effects on the small-signal gain can be neglected in this experiment, they cannot be responsible for the drop of the experimental data below the theoretical prediction. A possible explanation is that a deactivation rate of the CO_2 (001) level is higher than that used in the analytical model. If this is the case, the discrepancies between theory and experiment in constant area duct G_0 measurements may not only be caused by flow disturbances but also by higher deactivation rates. As noted by Anderson,[1] the uncertainties in the kinetic rates can strongly affect the prediction of the small-signal gain.

Figures 2 and 3 show peak gains as high as 0.9 m^{-1}. Such values are comparable to those obtained by other authors, e.g., Anderson,[1,3] using minimum length contoured nozzles. Although these results are somewhat interesting, they are no surprise, since the theoretical model proposed by Anderson was quite capable of predicting the high gains throughout the nozzle. The only problem was the overestimation of the gain near the nozzle exit. To extend these results, a laser power extraction experiment[10] is being carried out by the authors.

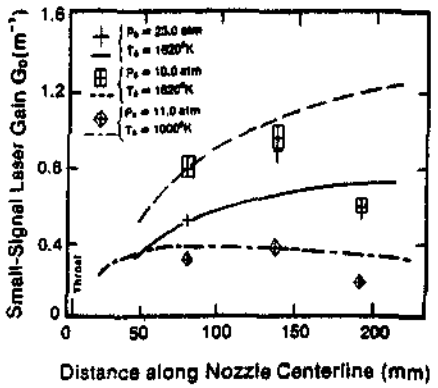

Fig. 3 Comparison between theoretical (lines) and experimental (points) small-signal laser gain profiles.

Conclusions

Small-signal gain measurements were conducted in a shock tube driven nonequilibrium expansion of a gas mixture containing 6.6% CO_2, 54.1% N_2, and 39.3% He at different reservoir conditions. The gain measurements were made at three locations downstream from the nozzle throat of a long double-wedge type hypersonic nozzle. The experimental results were compared with computer code predictions. The main results of this investigation are as follows:

1) Good agreement between the experimental data and the analytical predictions for the small-signal gain was obtained at the two stations closer to the nozzle throat.

2) Poor agreement between the experimental data and theoretical predictions for gain occurred at the station near the nozzle exit. At that location, the analytical model overestimates the actual gain. A possible reason could be the underestimation of the deactivation rate used by the theory.

3) Small-signal gain peaks of 0.9 m^{-1}, comparable with those obtained in minimum length contoured nozzles, were measured.

Acknowledgments

The authors wish to express their appreciation to the Brazilian Air Force for funding the present work. Particularly to Air Force Colonel Reginaldo dos Santos, director of the Instituto de Estudos Avançados, for his support and encouragement throughout this project. Thanks also to Sylvio Fish de Miranda for his valuable help at the laboratory during the tests. Acknowledgment is also due to Henry T. Nagamatsu and Leik N. Myrabo, from Rensselaer Polytechnic Institute, for their extremely useful advice and suggestions during the review of this work.

References

[1]Anderson, J. D., Jr., *Gasdynamic Lasers: An Introduction*, Chap. 5, Appendix A, Academic, New York, 1976.

[2]Lee, G., "Quasi-One-Dimensional Solution for the Power of CO_2 Gasdynamic Lasers," *Journal of Physics of Fluids*, Vol. 17, No. 3, 1974, pp. 644–649.

[3]Anderson, J. D., Jr., Humphrey, R. L., Vamos, J. S., Plummer, M. J., and Jensen, R. E., "Population Inversions in an Expanding Gas: Theory and Experiment," Naval Ordnance Lab., White Oak, MD, NOLTR 71-116, 1971.

[4]Mitra, N. K., and Fiebig, M., "Viscous Nozzle Flows and CO_2 Gasdynamic Lasers," *Proceedings of the International Symposium on Gasdynamic and Chemical Lasers*, DFVLR Press, Köln, Germany, Oct. 1976, pp. 298–340.

[5]Buonadona, V. R., and Christiansen, W. R., "Gain Measurements of High Temperature CO_2 Laser Mixtures in Shock Tube Driven Flow," *Recent Developments in Shock Tube Research*, Stanford Univ. Press, Stanford, CA, 1973, pp. 174–183.

[6]Klosterman, E. L., and Hoffman, A. L., "A High Pressure Shock Tube Driven Gasdynamic Laser," *Recent Developments in Shock Tube Research*, Stanford Univ. Press, Stanford, CA, 1973, pp. 156–166.

[7]Nagamatsu, H. T., Geiger, R. E., and Sheer, R. E., Jr., "Hypersonic Shock Tunnel," *ARS Journal*, Vol. 29, May 1959, pp. 332–340.

[8]Glowacki, W. J., and Anderson, J. D., Jr., "A Computer Program for CO_2-N_2-H_2O Gasdynamic Laser Gain and Maximum Available Power," Naval Ordnance Lab., White Oak, MD, NOLTR 71-210, 1971.

[9]Minucci, M. A. S., "Gain Measurements in a CO_2 CW Gas Dynamic Laser," M. Sc. Thesis, Inst. Tecnológico de Aeronáutica, Dept. of Aeronautical Engineering, S. J. dos Campos, São Paulo, Brazil, Dec. 1986 (in Portuguese).

[10]Minucci, M. A. S., and Hinckel, J. N., "Laser Gain Profiles During the Nonequilibrium Expansion of a CO_2-N_2-He System Through a Long Double-Wedge Type Hypersonic Nozzle," AIAA Paper 90-1511, June 1990.

Derivation and Testing of a One-Equation Model Based on Two Time Scales

U. C. Goldberg*
Rockwell International Science Center, Thousand Oaks, California 91360

Introduction

TURBULENCE measurements indicate that large-scale energy generating eddies possess a development rate substantially different from that of small-scale dissipative eddies. This suggests using a model that treats these eddies separately, assigning each range its own time scale. In the present work, a one-equation model is developed wherein the velocity scale is determined from the solution of an equation for the turbulence kinetic energy and the length scale is found indirectly from two time scales assigned each to large and small eddies. The derivation of this model leads to an expression for the near-wall function f_μ used in low Reynolds number versions of the k-ϵ model. A backflow model[1] is applied in conjunction with the one-equation model for the treatment of detached flow regions. Several flow cases are calculated to test the performance of this turbulence model.

Model Formulation

To account separately for the large (energy producing) eddies and the small (dissipative) eddies, characteristic time scales are assigned to each. Thus, the large eddies are characterized by

$$t_k \sim k/\epsilon \tag{1}$$

where k is the kinetic energy of the turbulence $k = \frac{1}{2}\overline{u_i' u_i'}$, and ϵ is the dissipation rate of k.

The small eddies are characterized by the Kolmogorov scale

$$t_\epsilon \sim \sqrt{\nu/\epsilon} \tag{2}$$

where ν is the kinematic molecular viscosity.

To determine these time scales, k and ϵ must be known throughout the flowfield. In the present work k is determined from the solution of a partially modeled version of the exact equation for turbulence kinetic energy

$$\frac{\partial}{\partial t}(\rho k) + \frac{\partial}{\partial x_i}(\rho U_i k) = \frac{\partial}{\partial x_i}\left[\left(\mu + \frac{\mu_t}{\sigma_k}\right)\frac{\partial k}{\partial x_i}\right] - \overline{\rho u_i' u_j'}\frac{\partial U_i}{\partial x_j} - C_k\frac{(\rho k)^2}{\mu_t} \tag{3}$$

Received Aug. 15, 1990; revision received Sept. 10, 1990; accepted for publication Sept. 18, 1990.

*Member Technical Staff. Member AIAA.

General Search Results--Full Record

Article 2 of 3 PREVIOUS NEXT SUMMARY FIND RELATED RECORDS Explanation

LASER GAIN MEASUREMENTS IN A LONG NONCONTOURED HYPERSONIC NOZZLE

MINUCCI MAS, **HINCKEL JN**

AIAA JOURNAL
29 (8): 1335-1337 AUG 1991

Document type: Note **Language:** English **Cited References:** 10 **Times Cited:** 0

Addresses:
CTR TECN AEROESP,SAO JOSE CAMPOS,BRAZIL
INST PESQUISAS ESPACIAS,SAO JOSE CAMPOS,BRAZIL

Publisher:
AMER INST AERONAUT ASTRONAUT, RESTON

IDS Number:
FZ251

ISSN:
0001-1452

Article 2 of 3 PREVIOUS NEXT SUMMARY

General Search Results--Full Record

Estimation of aerosol **transport from biomass burning areas during the SCAR-B experiment**

Trosnikov IV, **Nobre CA**

JOURNAL OF GEOPHYSICAL RESEARCH-ATMOSPHERES
103: (D24) 32129-32137 DEC 27 1998

Document type: Article **Language:** English **Cited References:** 11 **Times Cited:** 2

Abstract:
A transport model for the estimation-of tracers spreading from biomass burning areas has been developed on the basis of the semi-Lagrangian technique. The model consists of a three-dimensional Lagrangian form transport equation for tracers and uses the quasi-monotone local cubic-spline interpolation for calculation of unknown values at irregular points. A mass-conserving property of the model is based on the flux-corrected transport method using the algorithm of Priestley. The transport of the smoke particles from Amazonia was simulated for the period from August 20 to 29, 1995. During this period the air mass located below 2 km moved to the south and carried the smoke particles until 30 degrees S.

KeyWords Plus:
SCHEMES

Addresses:
Trosnikov IV, INPE, CPTEC, Ctr Weather Forecast & Climate Studies, Natl Inst Space Res, Rodovia Presidente Dutra, Km 40, BR-12630000 Cachoeira Paulista, SP, Brazil.
INPE, CPTEC, Ctr Weather Forecast & Climate Studies, Natl Inst Space Res, BR-12630000 Cachoeira Paulista, SP, Brazil.

Publisher:
AMER GEOPHYSICAL UNION, WASHINGTON

IDS Number:
155VL

ISSN:
0747-7309

JOURNAL OF GEOPHYSICAL RESEARCH, VOL. 103, NO. D24, PAGES 32,129-32,137, DECEMBER 27, 1998

Estimation of aerosol transport from biomass burning areas during the SCAR-B experiment

Igor V. Trosnikov and Carlos A. Nobre

Centro de Previsão de Tempo e Estudas Climáticos, Instituto Nacional de Pesquisas Espaciais, Chahoeira Paulista, SP, Brasil

Abstract. A transport model for the estimation of tracers spreading from biomass burning areas has been developed on the basis of the semi-Lagrangian technique. The model consists of a three-dimensional Lagrangian form transport equation for tracers and uses the quasi-monotone local cubic-spline interpolation for calculation of unknown values at irregular points. A mass-conserving property of the model is based on the flux-corrected transport method using the algorithm of Priestley. The transport of the smoke particles from Amazonia was simulated for the period from August 20 to 29, 1995. During this period the air mass located below 2 km moved to the south and carried the smoke particles until 30°S.

1. Introduction

The Smoke, Clouds, and Radiation - Brazil (SCAR-B) experiment was conducted in central Brazil and the southern Amazon Basin from August 15 to September 20, 1995, in collaboration with U.S. and Brazilian agencies and academic institutions [*McDougal*, 1995]. The aim of the experiment was to study the properties of aerosol and the effects of biomass burning on regional and global climate, including estimation of the emission product transport. In this study a numerical transport model has been developed on the basis of semi-Lagrangian technique [*Staniforth and Côté*, 1991] to estimate the dispersion of gas and aerosol emissions from an area with intense biomass burning. The model has been used for the estimation of aerosol transport during the SCAR-B experiment.

2. Model

The model is based on the three-dimensional Lagrangian form transport equation for tracers [*Brasseur and Madronich*, 1992]:

$$\frac{d\chi}{dt} = D_\chi + \frac{S_\chi}{\rho}, \qquad (1)$$

where d/dt is the material derivative, $\chi = \frac{\rho_\chi}{\rho}$ is the mixing ratio of the tracer with mass density ρ_χ, ρ is the air mass density, $D_\chi = K_H \nabla^2 \chi$ is the term of horizontal macrodiffusion, K_H is constant, and S_χ is the source term (expressed in mass per unit volume and time). This includes both positive and negative contributions. The lateral boundary conditions for equation (1) are taken to be $\chi = 0$ for boundary points with an influx of air.

For the integration of equation (1) the semi-Lagrangian technique is used. Every time step consists from two stages. The first stage is to find a solution of the trajectory problem: determine the departure points at time $t - \Delta t$ for arrival points of regular mesh at time t by using the known fields for these instants. They are determinated by a solution of the system of the equations

$$\frac{dx}{dt} = u, \quad \frac{dy}{dt} = v, \quad \frac{dz}{dt} = w - v_{sed} \qquad (2)$$

with the conditions

$$x(t) = x_a, \quad y(t) = y_a, \quad z(t) = z_a \qquad (3)$$

where u, v, w are the zonal, meridional, and vertical components of the wind velocity, v_{sed} is velocity of the sedimentation of the aerosol particles, and x_a, y_a, z_a are the regular mesh coordinates (arrival point). The system is integrated backward in time by the Crank-Nicolson scheme [*Williamson and Rash*, 1989]:

$$x_d(t - \Delta t) = x_a(t) - \frac{\Delta t}{2}(u_a(t) + u_d(t - \Delta t)), \qquad (4)$$

where Δt is a time step. The a index indicates known values, d index indicates unknown values which are determined by iterations. The same equations are integrated for y and z. The second stage consists of computations of the values of tracers on departure points and the sources of tracers on arrival points:

$$\chi_a(t) = \chi_d(t - \Delta t) + \Delta t \left(D_{\chi,a}(t - \Delta t) + \frac{S_\chi}{\rho} \right). \qquad (5)$$

The unknown wind components and the values of tracers for the departure points are obtained by the quasi-monotone local cubic-spline interpolation (see [*Bermejo and Staniforth*, 1992]). If a departure point is out of the integration area of the model, the boundary

Paper number 98JD01343.
0148-0227/98/98JD-01343$09.00

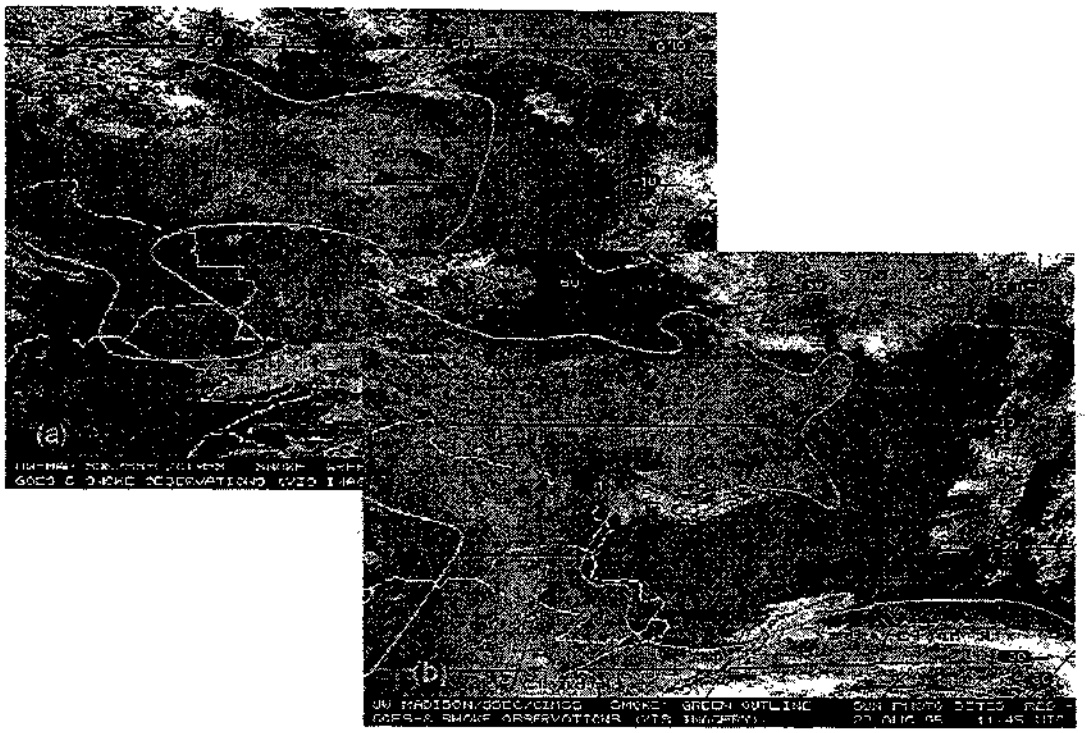

Figure 1. GOES-8 visible image of smoke concentration (a) at 1145 UTC, August 20, 1995, and (b) at 1145 UTC, August 29, 1995.

values are used. The value of the tracer is set equal to zero for arrival points located below the surface of the Earth.

3. Conservation

A conservation algorithm has been designed by using ideas from the flux-corrected transport (FCT) method [*Priestley*, 1993]. The solution of the transport equation for each point with index k is obtained from two approximations of the solution at the new time level, the high-order solution, χ_k^H, obtained by cubic interpolation, and the low-order solution, χ_k^L, obtained by linear interpolation,

$$\chi_k^M = \alpha_k \chi_k^H + (1 - \alpha_k)\chi_k^L \tag{6}$$

$$0 \le \alpha_k \le 1 \tag{7}$$

where α_k are to be chosen such as to make the conservative scheme for volume V

$$\int_V \chi^M(t)\rho(t)dxdydz = C \tag{8}$$

where value C includes the three terms

$$C = C_1 + C_2 + C_3\ , \tag{9}$$

C_1 is the aerosol mass for the time moment $t - \Delta t$, C_2 and C_3 are the aerosol mass injected in the atmosphere by sources and the aerosol flux through the lateral boundary consequently on the time interval $(t - \Delta t, t)$:

$$C_1 = \int_V \chi^M(t - \Delta t)\rho(t - \Delta t)dxdydz \tag{10}$$

$$C_2 = \Delta t \int_V S_\chi dxdydz \tag{11}$$

$$C_3 = \Delta t \int_\Omega \rho\chi^M(t - \Delta t)\mathbf{n}\mathbf{v}(t - \Delta t)d\Omega, \tag{12}$$

$\mathbf{n}$ is the inside normal to the lateral boundary Ω. When the sources and flux through the lateral boundary are absent, the mass of aerosol is conservation value. The Priestley algorithm is used for determination of α_k by minimization of the difference between χ^M and χ^H with condition (8).

4. Simulation of Aerosol Transport for SCAR-B Experiment

For the simulation of aerosol transport, the analysis fields of the wind, temperature, and geopotential height produced by the CPTEC global numerical weather forecast model and available from SCAR-B database were used. The grid of the analyses has 49 x 41 points with a horizontal resolution of 1.875°x1.875° and covers South America from 101.25°W to 26.25°W and from 60°S to 15°N. The transport model has the horizontal grid colo-

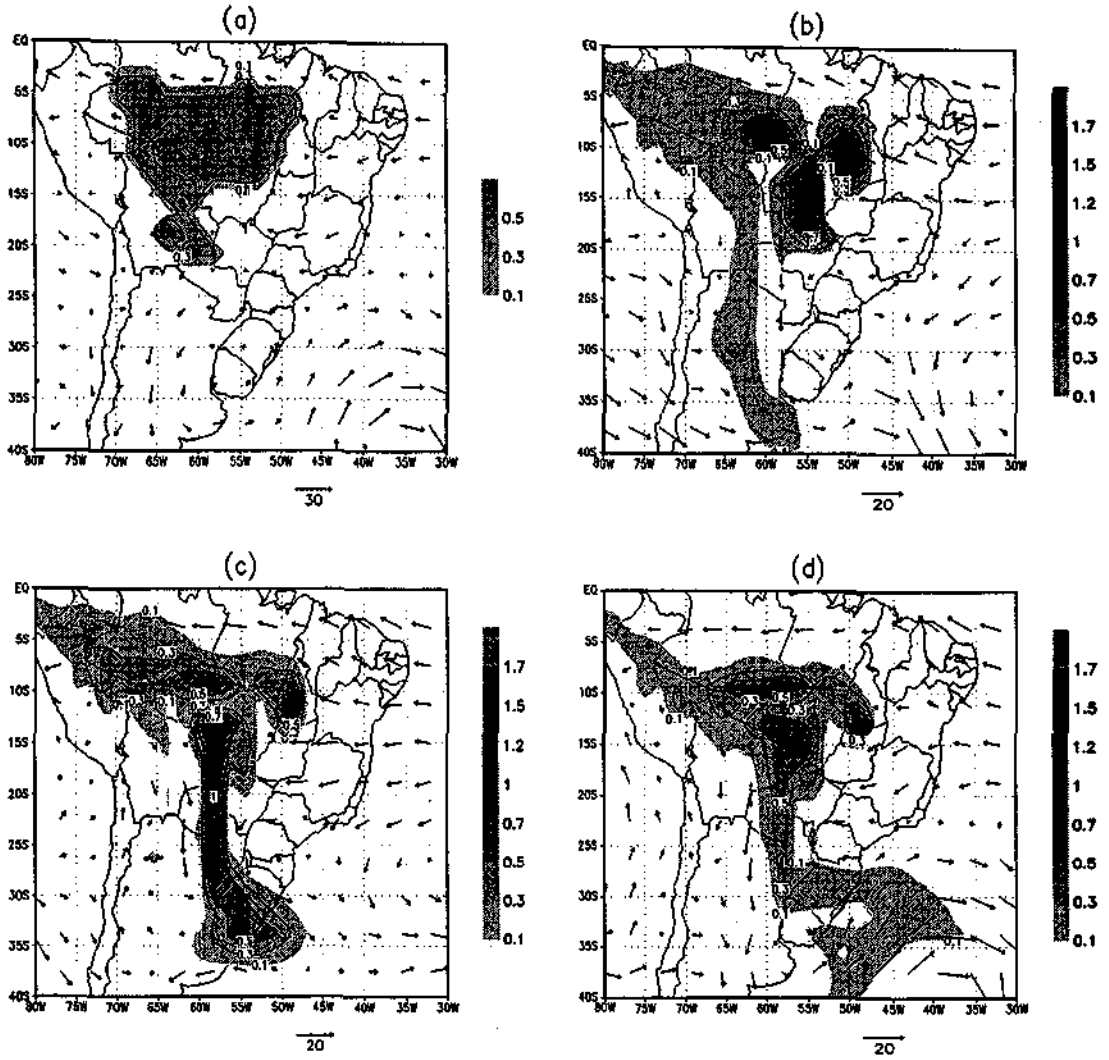

Figure 2. Simulated aerosol concentration (arbitrary units) and wind (m s^{-1}) at 850 hPa: (a) August 20, 1995 (initial condition); (b) August 23, 1995; (c) August 26, 1995; (d) August 29, 1995.

cated with the analyses grid, and its vertical structure includes 22 pressure levels from 1000 to 200 hPa, 16 of which are placed in the layer 1000-700 hPa. The time integration of the model was carried out with a 1 hour time step, and hourly values of the meteorological elements were calculated by linear interpolation.

4.1. Location of Aerosol Sources in Separate Regions

The sources of the aerosol $S(x, y, z)$ were set in the grid points and were defined by two parameters: the intensity of the aerosol injection to the atmosphere S_0(g m^{-2} s^{-1}) and the total thickness of the source layer ΔP(hPa). The simple vertical change source model was used:

$$\frac{S}{\rho} = \frac{gS_0}{100\Delta P}, \tag{13}$$

where ΔP is the thickness of the air layer with the source in hPa, and g is the gravitational acceleration. The choice of ΔP for numerical experiments was determined by SCAR-B data, which shows layers of high aerosol concentrations at 1800-2500 m altitude [*Artaxo et al.*, 1996].

The aerosol measurements during the SCAR-B experiment show that aerosol particles have a size distribution with a mass peak at about 0.3 μm diameter [*Artaxo et al.*, 1996]. It allows one to use the bulk representation of aerosol particles for transport calculations as the first approximation. The velocity of the sedimentation was taken to be 0.001 ms^{-1} [*Penner et al.*, 1991a] according to this approximation. Because the calculations were carried out for a dry season, wet scavenging is not included in the source.

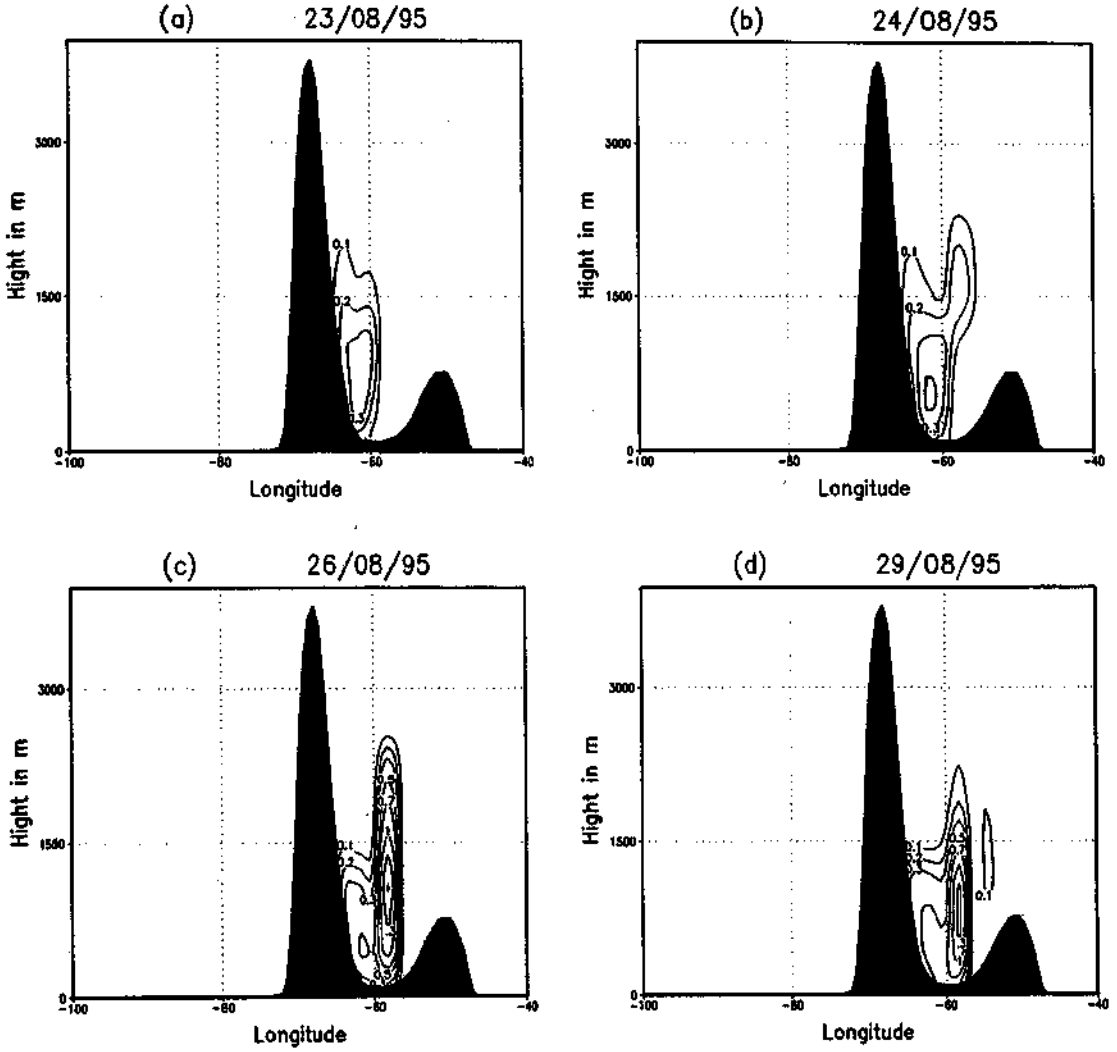

Figure 3. Simulated aerosol concentration cross section (arbitrary units) along 25°S: (a) August 23, 1995; (b) August 24, 1995; (c) August 26, 1995; (d) August 29, 1995.

The preliminary computations showed that the term of horizontal macrodiffusion in equation (1) leads to a marked increase of the aerosol spreading area. For this reason the simulation of aerosol transport for the SCAR-B experiment was conducted with $K_H = 0$.

In the first numerical experiments the following source parameters were used: ΔP = 162.5 hPa or the source height was about 1500 – 2000 m, S_0=7.5 × 10^{-6} g m^{-2} s^{-1}.

To link S_0 with S_f, the intensity of the aerosol injection to the atmosphere from a fire territory with the area A_f, the relation

$$S_0 A_g = S_f A_f \tag{14}$$

can be used, where A_g is the model grid cell area. For example, for S_f=0.003 g $m^{-2}s^{-1}$ [*Penner et al.*, 1991b] and A_g=41500.0 km^2, the fire area is A_f=103.8 km^2.

The first simulation of the aerosol spreading from four separate fire regions during the period from August 20 to 29, 1995, is demonstrated (Figures 2 and 3). The centers of the regions were placed at the points with coordinates (1) 56°W, 9.5°S (the region of Alta Floresta); (2) 52°W, 18.5°S (between Campo Grande and Brasília); (3) 55°W, 17°S (between Campo Grande and Cuiabá); and (4) 48.5°W, 13.5°S (between Porto Nacional and Brasília). The initial conditions for the smoke concentration were set quasi-uniformly with the average density in the atmospheric column about of 0.06 g m^{-2} and the geographic configuration subjectively extracted from the GOES-8 visible image at 1145 UTC on August 20, 1995 (see Figures 1a and 2a). As shown in Figures 2a and 2b, from August 20 to 23, 1995, initially, the simulated aerosol moved westerly from the Alta Floresta region and southerly from northern Paraguay. By

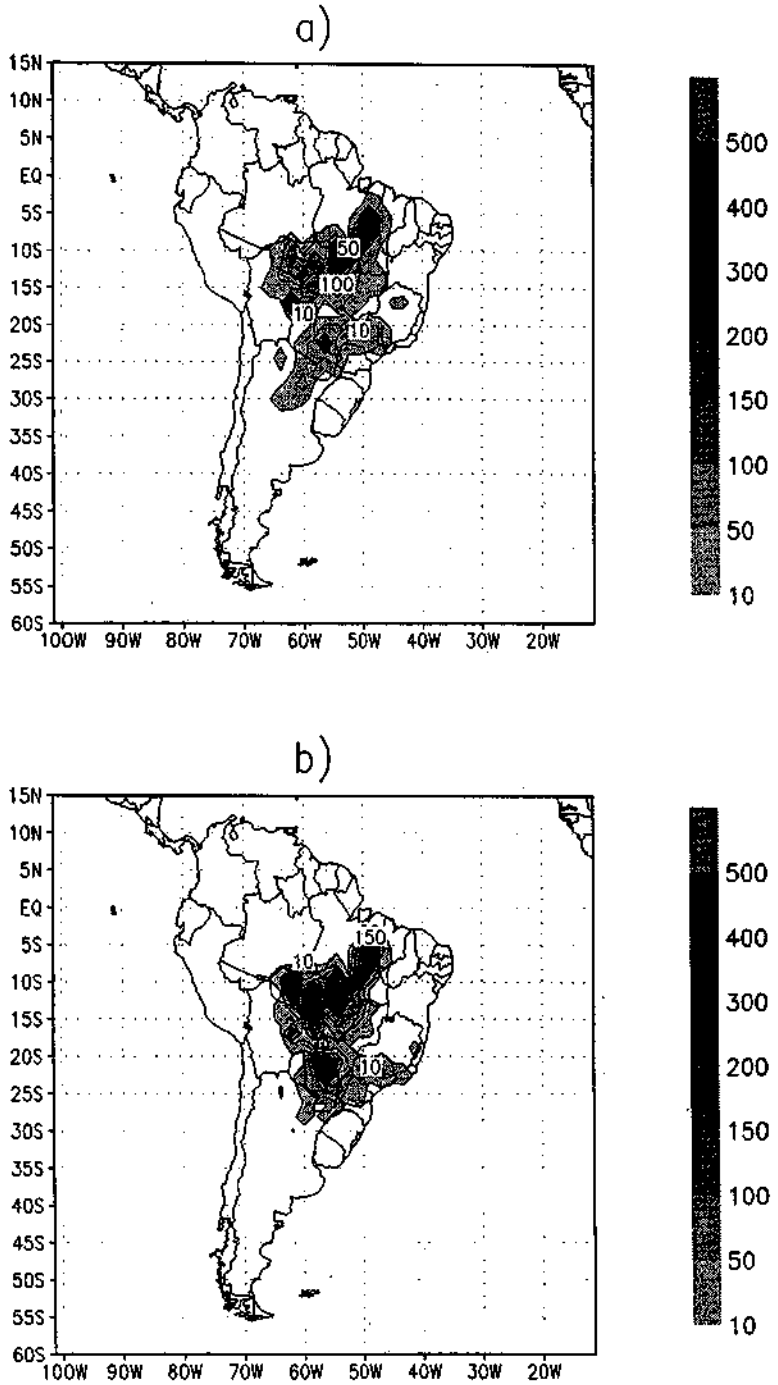

Figure 4. Cumulative weekly number of fires in the model grid cells (a) for August 18-24, and (b) for August 25 - 31, 1995.

August 29 it reached 35°S. The locations of the different aerosol sources are better seen in Figure 2b. After August 23, 1995, the simulated aerosol began to spread southerly from the Cuiabá region and formed a narrow current which arrived at the latitude belt of 30°S-35°S (see Figure 2c).

The vertical structure of the southerly simulated aerosol currents can be seen in the vertical cross sections of the aerosol concentration along 25°S in Figure 3. Figure 3a shows a cross section of the simulated aerosol current which includes aerosol particles from the Randonia region. In Figure 3b one can see the additional simulated

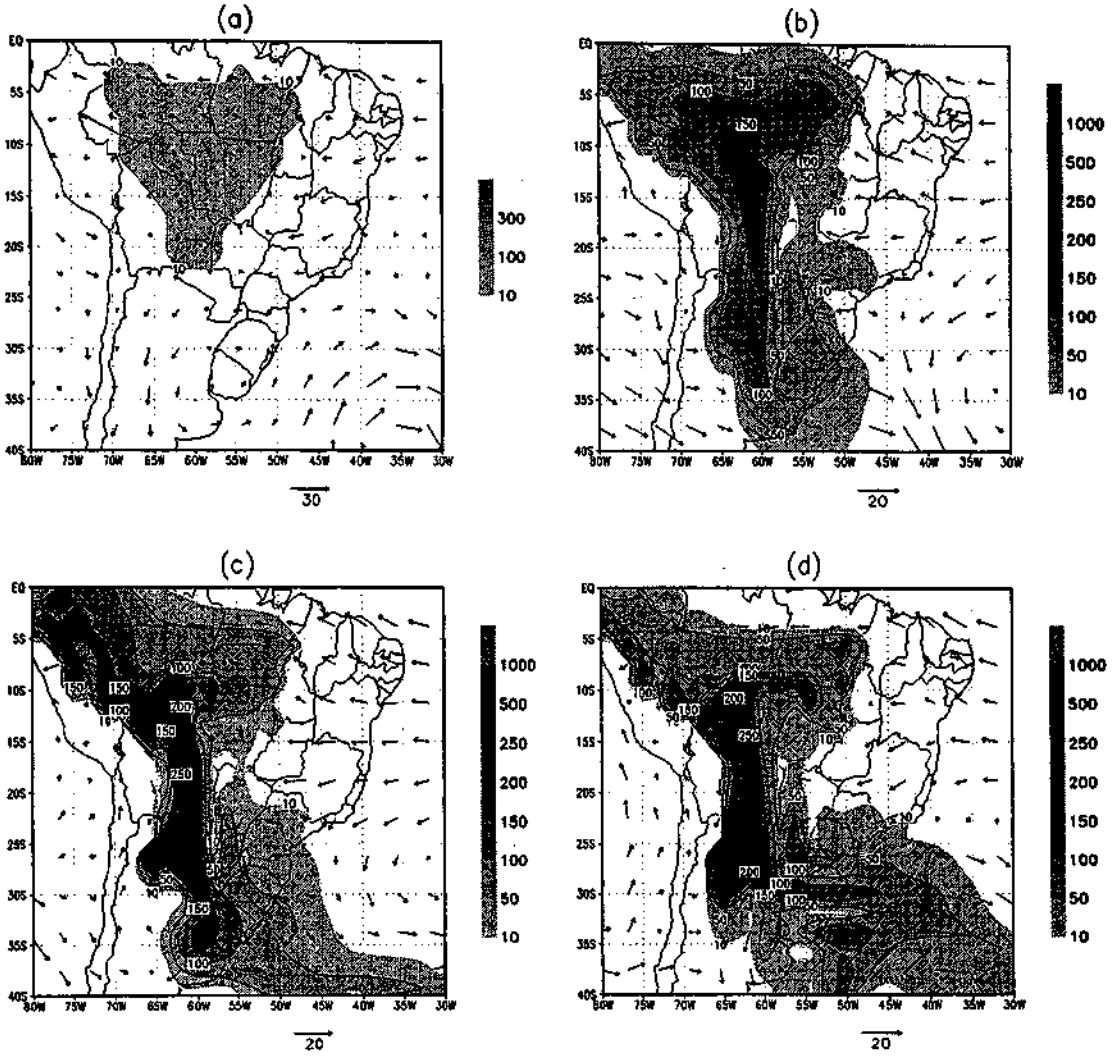

Figure 5. Simulated aerosol concentration (μg m^{-3}) and wind (m s^{-1}) at 850 hPa: (a) August 20, 1995 (initial condition); (b) August 23, 1995; (c) August 26, 1995; and (d) August 29, 1995, for the experiment with location of the aerosol sources in the burning areas.

aerosol current from the Cuiabá region. Figures 3c and 3d show the evolution of these simulated aerosol currents. On account of sedimentation, aerosol particles have the marked redistribution of heights depending on their lifetime in the atmosphere.

4.2. Location of Aerosol Sources in Burning Areas

For determination of the burning areas during the SCAR-B period, data of the NOAA operational satellite monitoring of fires have been used. The fire monitoring data are produced by the National Institute for Space Research/INPE (Brazil) and include cumulative weekly number of fires in grid cells of 0.5° latitude by 0.5° longitude. The data were used for 2 weeks, August 18-24 and 25-31, 1995. The data have been remapped onto the model cells (see Figure 4). The fire numbers have been used for the determination of aerosol sources in the model grid points

$$\frac{S}{\rho} = \frac{gS_0}{100\Delta P} w(\lambda, \varphi, t)\,, \tag{15}$$

where $S_0 = 2.25 \times 10^{-6}$ g m^{-2} s^{-1}, ΔP=300 hPa, and $w(\lambda, \varphi, t)$ is the dimensionless weight function proportional to the number of fires in the model grid point k, n_k,

$$w_k = \frac{n_k}{\max_j(n_j)}\,. \tag{16}$$

The value of w lies in the limits: $0.03 < w \leq 1$.

Figure 5 shows the time evolution of the simulated aerosol concentration in μg m^{-3} on the pressure level 850 hPa. One can see that the principal features of the aerosol spreading are consistent with the aerosol spreading from the separate sources in the first experiment.

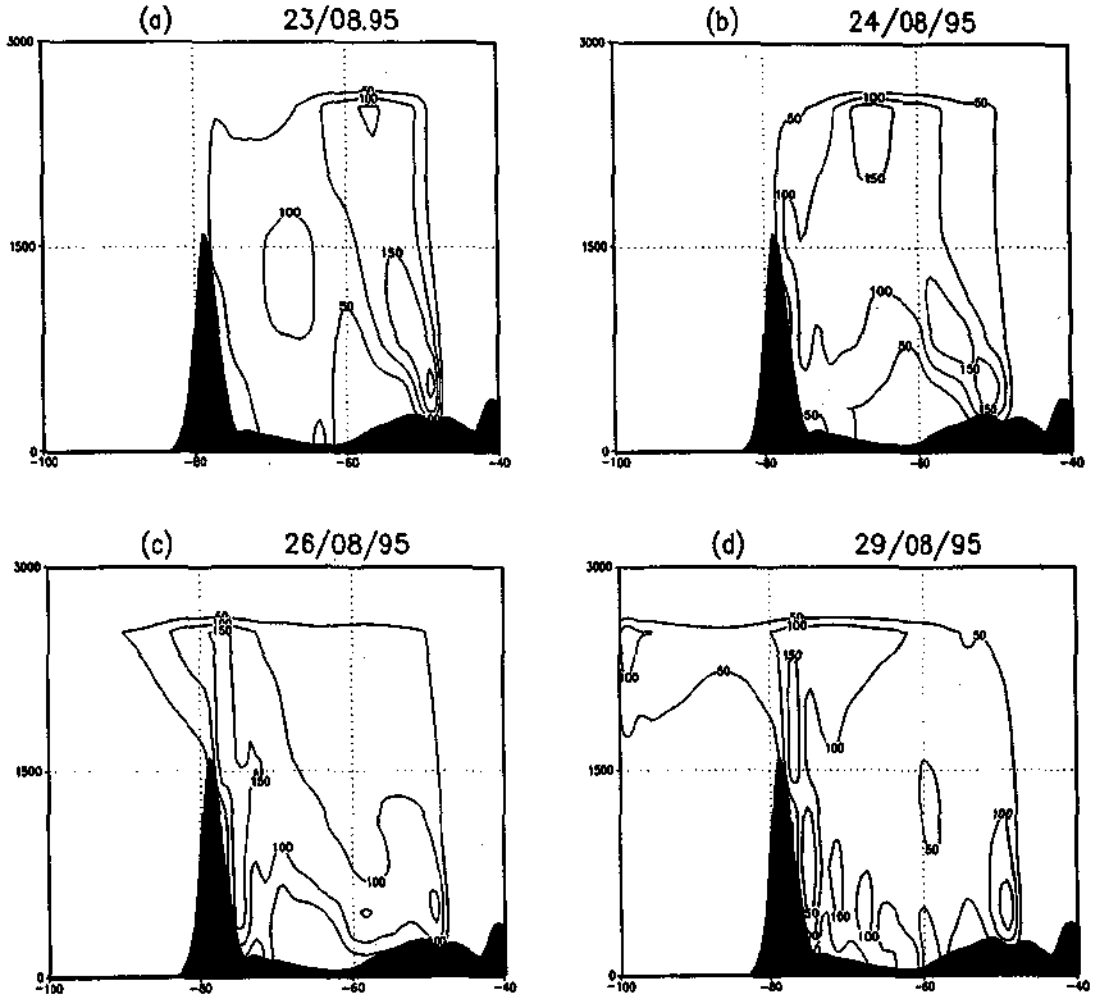

Figure 6. Simulated aerosol concentration cross section (μg m^{-3}) along 5°S: (a) August 23, 1995; (b) August 24, 1995; (c) August 26, 1995; (d) August 29, 1995 for the experiment with location of the aerosol sources in the burning areas.

The main difference is that aerosol was also carried from the continent to the Pacific Ocean in the latitude belt from 5°S to 5°N. The vertical structure of this current is shown in Figure 6 for the vertical cross section of the simulated aerosol concentration in μg m^{-3} along 5°S. It should be noted that the values of the aerosol concentration are close to the observed values during the SCAR-B experiment [*Artaxo et al.*, 1996].

To estimate the aerosol amount for the second experiment, the components of the aerosol balance have been calculated. They are represented in Table 1. shows the time evolution of the simulated aerosol co The total aerosol emission, 3.143 Tg, during 10 days, can be compared with annual aerosol emission in tropical America, 22.0 Tg [*Penner et al.*, 1991a].

4.3. Estimation of Optical Depth

The quantity of the total aerosol mass in the atmospheric column $m = \frac{1}{g}\int \chi \rho dp$ can be related to optical depth τ by

$$\tau = \gamma m, \tag{17}$$

where γ is a specific extinction coefficient. The optical depth values may be compared with observations. The value of γ=2.73 m^2 g^{-1} has been derived for the spectral channel 0.67 μm from measured physical characteristics (mass scattering and absorption efficiency, and single-

Table 1. Components of Aerosol Mass Balance for Experiment With Source Locations in Burning Areas

Component	1995	Value	Units
Initial aerosol mass	August 20	0.6930	Tg
Total Aerosol Emission	August 21-29	3.1433	Tg
Total Aerosol Flux Through Boundaries	August 21-29	-0.5679	Tg
Aerosol Mass	August 29	3.2684	Tg

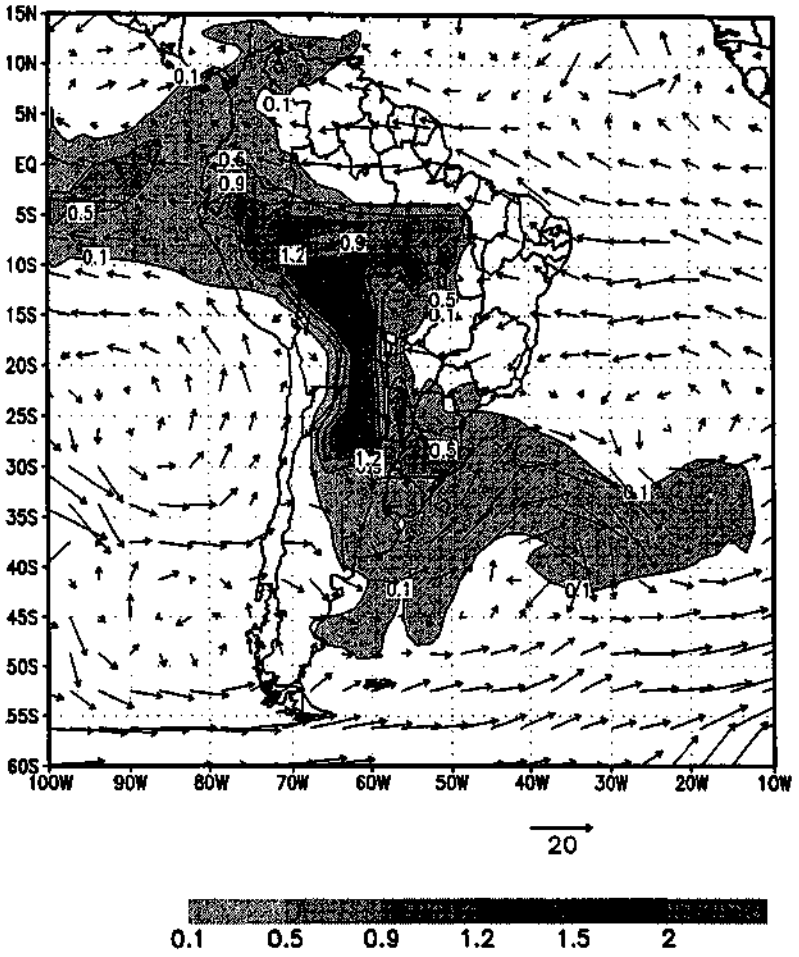

Figure 7. Optical depth of the aerosol on the surface on August 29, 1995, for the experiment with location of the aerosol sources in the burning areas.

scattering albedo) in regional hazes in Brazil during the SCAR-B experiment [*Reid et al.*, 1996]. Figure 7 shows the estimated optical depth of the aerosol for August 29, 1995. The calculated values are similar to the values of the observations for biomass burning periods [*Kaufman et al.*, 1992]. The calculated large-scale pattern of the aerosol distribution for August 29, 1995, shows a good agreement with the observed haze on GOES-8 visible image (see Figure 1b). However, the agreement of the calculated and observed values of the optical depth for local points is not so good. Table 2 shows the (1) model estimated and (2) observed optical depth for the three stations. The observed data have been taken from the AERONET (Aerosol Robotic Network) data archive.

Table 2. Model Estimated and Observed Optical Depth Values for Stations From August 22 to 29, 1995

	August 1995							
Station	22	23	24	25	26	27	28	29
Alta Floresta								
a	1.30	0.95	0.83	0.95	1.11	1.20	1.20	1.32
b	1.18	1.88	1.13	1.11	1.12	1.26	1.30	1.34
Brasília								
a	0.04	0.04	0.04	0.02	0.02	0.02	0.03	0.02
b	0.08	–	0.08	0.08	0.07	0.06	0.08	0.09
Cuiabá								
a	0.06	0.13	0.16	0.09	0.09	0.11	0.12	0.16
b	0.11	0.04	0.12	0.06	0.17	0.08	–	0.37

The a is model estimated and b is observed optical depth values.

Although the optical depth level was simulated correctly for the stations, there is a discrepancy between estimated and observed small optical depths. It may be linked with the formation of aerosol density for Brasília and Cuiabá stations by local small-scale sources during August 22-29, 1995.

5. Conclusions

The transport model for the estimation of tracers from biomass burning areas has been developed on the basis of the semi-Lagrangian technique. The model includes principal processes which form large-scale tracer spreading for dry season: horizontal and vertical advection, sedimentation of aerosol particles, and horizontal turbulent exchange. No vertical diffusion is included in the model because poor boundary layer large-scale analysis data have been used for aerosol transport computation. They do not make it possible to estimate good parameters of the convective boundary layer. In fact, for burning areas the vertical turbulent exchange was added in the transport model by a source term (equation (15)) which includes full complex subgrid vertical transport from the surface to the atmosphere. The model has the property of tracer mass conservation that permits its use for balance calculations.

The simulation of the aerosol spreading for the SCAR-B period from August 20 to 29, 1995, showed that the air mass located below 2 km moved mainly to the south and carried the smoke until 30°S. A similar transport of the aerosol is observed on the GOES-8 satellite images. Another significant transport of aerosol was from the Alta Floresta region to the northwest.

Although the model seems to have realistically captured the geographical distribution of aerosol emanating from biomass burning areas during SCAR-B, it still needs improvement to represent the quantitative distribution of optical depth.

Acknowledgments. We thank three anonymous reviewers for their constructive comments. This research has been sponsored by CNPq (Brazil).

References

Artaxo, P., E. T. Fernandes, J. V. Martins, M. A. Yamasoe, K. M. Longo, P. V. Hobbs, and W. Maenhaut, Large scale elemental composition of aerosols measured during SCAR-B, in *SCAR-B Proccedings: Collection of Papers at the Fortaleza, Brazil, Workshop*, edited by V. W. J. H. Kirchhoff, pp. 9-14, Transtec, São Jose dos Campos, São Paulo, Brazil, 1996.

Bermejo, R., A. Staniforth, The conversion of semi-Lagrangian advection schemes to quasi-monotone schemes, *Mon. Weather Rev., 120,* 2622-2632, 1992.

Brasseur, G. P., and S. Madronich. Chemistry-transport models, in *Climate System Modeling*, edited by K. E. Tremberth, chap. 15, Cambridge University Press, New York, 1992.

Kaufman, Y.J., A. Setzer, D. Ward, D.Tanre, B. N. Holben, P. Menzel, M. C. Pereira, and R. Rasmussen, Biomass Burning Airborne and Spaceborne Experiment in the Amazonas (BASE-A), *J. Geophys. Res., 97,* 14,581-14,599, 1992.

McDougl, D., Smoke, Clouds and Radiation-Brazil (SCAR-B) field experiment, August 16 to September 14, 1995, Mission Plan, prepared by SCAR-B scientists and the SCAR-B Project Office, *NASA spec. publ.*, 164 pp., 1995.

Penner, J.E., S.J.Ghan, and J.J.Walton, The role of biomass burning in the budget and cycle of carbonaceous soot aerosols and their climate impact, in *Global Biomass Burning: Atmospheric, Climate, and Biospheric Implication*, edited by J. S. Levine, pp. 387-393, MIT Press, Cambridge, Mass., 1991a.

Penner, J.E., M.M. Bradley, C.C. Chuang, L.L. Edwards, and L.F. Radke. A numerical simulation of the aerosol-cloud interactions and atmospheric dynamics of the Hardiman Township, Ontario, prescribed burn, in *Global Biomass Burning: Atmospheric, Climate, and Biospheric Implication*, edited by J. S. Levine, pp. 420-426, MIT Press, Cambridge, Mass., 1991b.

Priestley, A., A quasi-conservative version of the semi-Lagrangian advection scheme, *Mon. Weather Rev., 121,* 621-629, 1993.

Reid, J. S., P. V. Hobbs, and R. J. Ferek. Physical and chemical characteristics of biomass burning aerosols in Brazil, in *SCAR-B Proccedings: Collection of Papers at the Fortaleza, Brazil, Workshop*, edited by V. W. J. H. Kirchhoff, pp. 165-169, Transtec, São Jose dos Campos, São Paulo, Brazil, 1996.

Staniforth, A., and J. Côté, Semi-Lagrangian schemes for atmospheric models – A review, *Mon. Weather Rev., 119,* 2206-2223, 1991.

Williamson, D., and P.Rasch, Two dimensional semi-Lagrangian transport with shape-preserving interpolation, *Mon. Weather Rev., 117,* 102-109, 1989.

C.Nobre and I. Trosnikov, Center for Weather Forecast and Climate Studies, National Institute for Space Research - CPTEC/INPE, Rodovia Presidente Dutra, km 40 - SP, CEP 12630-000, Cachoeira Paulista, SP, Brazil (e-mail: igor@cptec.inpe.br)

(Received September 9, 1997; revised April 3, 1998; accepted April 7, 1998.)